applied sciences

MDPI

Article

Flexural Behavior of Self-Prestressed RC Slabs with Fe-Based Shape Memory Alloy Rebar

Yeong-Mo Yeon, Ki-Nam Hong * and Sang-Won Ji

Department of Civil Engineering, Chungbuk National University, 1 Chungdae-ro, Seowon-Gu, Cheongju 28644, Korea; yym235@chungbuk.ac.kr (Y.-M.Y.); tkddnjs0727@chungbuk.ac.kr (S.-W.J.)
* Correspondence: hong@chungbuk.ac.kr

Abstract: A lot of studies have been conducted to introduce self-prestress to structures using Fe-based shape memory alloys (Fe-SMAs). Technology to introduce self-prestress using Fe-SMAs can resolve the disadvantages of conventional prestressed concrete. However, most of the research to introduce a self-prestress force to a structure using Fe-SMAs has been focused on using Fe-SMAs for the repair and strengthening of aging structures. Therefore, in this paper, a study was conducted to introduce self-prestress into a new structure. To this end, in this paper, an experimental study was conducted to evaluate the flexural behavior of self-prestressed concrete slabs with Fe-SMA rebar. Nine specimens were built with consideration of the amount and activation of Fe-SMA rebars as experimental variables. The Fe-SMA rebars used in the specimens exhibited recovery stress of about 335 MPa under the conditions of a pre-strain of 0.04 and a heating temperature of 160 °C. Activation of the Fe-SMA rebars by electrical resistance heating applied an eccentric compression force to the specimen to induce a camber of 0.208–0.496 mm. It was confirmed through a 4-point bending test that the initial crack loads of the activated specimens were 40~101% larger than that of the non-activated specimens. However, the ultimate loads of the activated specimens showed a difference within 3% from that of the non-activated specimens, confirming that the effect of activation on improving the ultimate strength was negligible. Finally, it was confirmed that repetitive activation of the Fe-SMA rebar could repeatedly apply compressive force to the slab.

Keywords: shape memory alloy; recovery stress; initial crack; self prestressing; camber

Citation: Yeon, Y.-M.; Hong, K.-N.; Ji, S.-W. Flexural Behavior of Self-Prestressed RC Slabs with Fe-Based Shape Memory Alloy Rebar. *Appl. Sci.* **2022**, *12*, 1640. https://doi.org/10.3390/app12031640

Academic Editors: Deuckhang (DK) Lee, Sung-Woo Moon, Donghyuk Jung and Sanghee Kim

Received: 12 January 2022
Accepted: 3 February 2022
Published: 4 February 2022

1. Introduction

Prestressed concrete is structural concrete in which internal stress is introduced using tendons in areas where tensile stress resulting from the external load is likely to occur. The internal stress can effectively control the occurrence of cracks by offsetting the tensile stress caused by the external load [1,2]. Therefore, since prestressed concrete is recognized as being effective in resisting the load, the size of the cross-section and its self-weight can be reduced compared with a reinforced concrete (RC) member [3]. The prestressed method can be broadly divided into pre-tension and post-tension methods [4]. The pre-tension method is a method in which the tendons are tensioned before concrete is poured. In this method, the bonding force between the concrete and the tendon resists the recovery of elastic deformation of the tendon released after curing of the concrete and consequently acts as a compressive force on the cross-section. Because bulkheads are required in the process of introducing prestress with this method, this method is mostly used in precast concrete (PC) factories rather than on-site [5]. On the other hand, the post-tension method entails tensioning and anchoring the tendon after the concrete has been cured [6]. Unlike the pre-tension method, it can be easily applied in the field because separate support is not required. For this reason, the post-tension method is widely used in large-scale construction works such as long-span bridges [7]. Prestressed concrete manufactured by the post-tension method is classified into bonded prestressed concrete and unbonded prestressed

concrete [8]. In bonded prestressed concrete, the concrete and the tendon work integrally by grouting the ducts after tensioning and anchoring the tendon [9]. However, the grouting operation complicates the construction process and increases the construction period. Moreover, the prestressing force of the bonded prestressed concrete cannot be recovered, even if it decreases due to various causes such as concrete creep, drying shrinkage, and tendon relaxation over time [10]. On the other hand, in unbonded prestressed concrete, the sheath pipe is not grouted after tensioning the tendon [11]. Unlike bonded prestressed concrete, the tendons of unbonded prestressed concrete can be re-tensioned when the prestressing force is reduced. However, unbonded prestressed concrete has lower strength and lower durability due to increased crack widths compared with bonded prestressed concrete [12].

Technology to introduce prestress using shape memory alloy (SMA) can resolve the aforementioned disadvantages of conventional prestressed concrete [13]. SMA is a metal with special properties where even if plastic deformation occurs, it can be recovered by the shape recovery effect (SME), which is triggered by activation consisting of heating and cooling [14]. When the pre-tensioned SMA is activated under restraint, the alloy tries to return to its original shape by the SME, but because it is restrained, compressive stress, referred to as recovery stress, occurs inside the alloy [15]. Similarly, when a pre-tensioned SMA embedded in concrete is heated by electric resistance heating, the SME will be exerted on the SMA toward shrinking it to its original state by the SME. However, the recovery of the SMA deformation is restrained by the bond between the SMA and concrete, resulting in the generation of recovery stress acting as a compressive force on the concrete [16]. This prestress introduction principle is similar to that of the pre-tension method, in which the bonding force between the concrete and the tendon resists the recovery of elastic deformation of the tendon released and acts as a compressive force on the cross-section. In addition, this method has the advantage of being easily applied in the field like the conventional post-tension method because separate support is not required. Concrete to which prestress is introduced in this way can have excellent mechanical performance because the SMA and concrete work integrally, similar to conventional bonded prestressed concrete. Moreover, unlike bonded prestressed concrete, the prestressing force of prestressed concrete using SMAs can be recovered through its reactivation, even if it is reduced by various causes. To date, more than 300 types of SMAs have been reported [17]. Among them, Ni-Ti-based SMA (Nitinol), developed by Buehler et al. [18] in 1963, is currently the most widely used because it shows excellent superelasticity and an SME [19]. However, Nitinol has a relatively narrow temperature history. Moreover, because it contains high-priced nickel and titanium in large proportions, Nitinol is not used as a construction material [20].

On the other hand, Fe-based shape memory alloy (Fe-SMA) has a lower manufacturing cost compared with Nitinol because iron is the main constituent material, and many researchers are studying it for use as a construction material. Shahverdi et al. [21] conducted an experimental study to use Fe-SMA strips as a strengthening material in conjunction with use of the NSM method. They evaluated the flexural performance of RC beams with Fe-SMA strips as reinforcement in the NSM method through a four-point loading test. They reported that the specimen with activated Fe-SMA exhibited a higher initial stiffness than the specimen with non-activated Fe-SMA through analysis of the test results. In addition, they argued that the cause was the action on the cross-section of the compressive force due to the activation of Fe-SMA. Shahverdi et al. [22] evaluated the mechanical properties, recovery properties, and relaxation of Fe-SMA in order to secure basic data for using Fe-SMA strips as strengthening materials for RC members. The alloy composition ratio of the Fe-SMA strip used in the study was Fe-17Mn-5Si-10Cr-4Ni-1(V,C) (mass %), and the specimen was 100 mm wide and 1.5 mm thick. They reported that when Fe-SMA was heated to 160 °C, a recovery stress of 300–350 MPa was generated, which was reduced by about 10% by relaxation after 1000 h. Abouali et al. [23] performed an analytical study to predict the flexural performance of RC members strengthened with Fe-SMA

by the NSM method. They presented a finite element analysis model of an RC member strengthened with Fe-SMA by the NSM method using a commercial structural analysis program. They compared the experimental results published by Shahverdi et al. [21] with the results predicted by the FE model in order to secure the reliability of the finite element analysis results. They also confirmed through a parametric analysis that the ductility of the RC beams strengthened with Fe-SMA increased as the concrete strength increased, and the initial stiffness of the RC beams increased by more than 60% when the Fe-SMA was activated.

As such, few studies on the use of Fe-SMA rebars in new structures have been reported. Most of the research to introduce a prestress force to a structure using Fe-SMA has been focused on using Fe-SMA for the repair and strengthening of aging structures [24–26]. In previous studies, a cementitious matrix or anchoring device was used to attach Fe-SMA rebars, plates, or strips to RC members. However, it is difficult to accurately evaluate the effect of Fe-SMA on the RC member because the behavior of the strengthening RC member is affected by the anchoring device and the bonding strength between the RC member and the cement matrix. In addition, previous studies evaluated the reactivation potential of Fe-SMA through material tests [27], and there are few studies testing the reactivation possibility of Fe-SMA used in the RC member. Therefore, this study conducts flexural tests on one-way RC slabs using Fe-SMA rebars as a tensile reinforcement and evaluates the effect of the prestressing force by Fe-SMA rebar on their flexural behavior. In addition, the possibility of reactivation of Fe-SMA was experimentally evaluated.

2. Materials and Methods

2.1. Test Specimens

Nine specimens were constructed to evaluate the flexural behavior of concrete slabs using Fe-SMA rebars. As shown in Figure 1, the section of the specimen was 400 mm wide and 250 mm high, and the concrete cover and the effective depth of the section were 35 mm and 210 mm, respectively. The total length of the specimens was 2800 mm, and their net span was set to 2600 mm. The Fe-SMA rebars used in the experiment had a 10 mm × 10 mm square cross-section. In order to prevent the Fe-SMA rebar from slipping during the experiment, a 100-mm long thread was machined to install the fixing device at both ends of the rebar. These rebars were tensioned to a target pre-strain of 0.04 by a horizontal tensioning device and assembled into a rebar mesh. After all preliminary work was completed, the specimens were cast. After that, the specimens were cured for 28 days through moist curing. Table 1 shows the test variables considered for the evaluation of the flexural behavior of concrete slabs using Fe-SMA rebars. The amount of the Fe-SMA rebar (200 mm^2, 300 mm^2, 400 mm^2, or 500 mm^2) and its activation were considered to be experimental variables. The variable name 'SL' in Table 1 denotes 'Slab', and Arabic numerals indicate the number of Fe-SMA rebars. In addition, the letters 'A', 'N', and 'R' after the Arabic number denote the activation, non-activation, and reactivation of the Fe-SMA bar, respectively.

Table 1. Test variables.

Specimen	Area of Fe-SMA Rebar (mm^2)	Activation
SL-2N	200	Non-activation
SL-2A		Activation
SL-3N	300	Non-activation
SL-3A		Activation
SL-3R		Re-activation
SL-4N	400	Non-activation
SL-4A		Activation
SL-5N	500	Non-activation
SL-5A		Activation

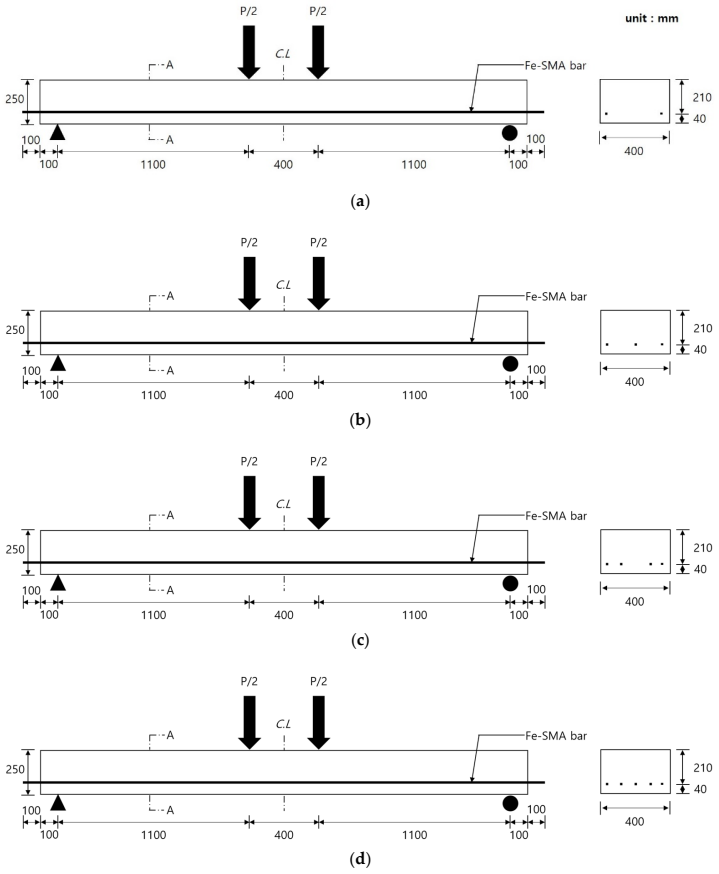

Figure 1. Details of the test specimens: (**a**) SL-2N and SL-2A, (**b**) SL-3N, SL-3A, and SL-3R, (**c**) SL-4N and SL-4A, and (**d**) SL-5N and SL-5A.

2.2. Materials

The concrete used in constructing the specimens was ready-mixed concrete, and the mixture design of the concrete is shown in Table 2. The design compressive strength, the water-to-cement ratio, and the cement type of the mixture with a 25-mm maximum aggregate size were 40 MPa, 30.7%, and type 1 ordinary Portland cement, respectively. Simultaneous with the concrete pouring, 5 cylinders with a size of Φ 100 mm × 200 mm were produced to measure the compressive strength of the concrete. The cylinders were demolded and cured under the same conditions as the specimens, and a compressive strength test was performed in accordance with the ASTM standard [28] on the testing date. Through the analysis of the test results, the average compressive strength of the concrete was determined to be 46.2 MPa.

Table 2. Test variables.

Slump (cm)	Air Content (%)	W/B (%)	S/a (%)	Weight Per Unit Volume (kg/m^3)				
				W	C	S	G	AD
12	4.5	30.7	47	192	625	684	780	4.38

The chemical composition ratio of the Fe-SMA rebar used in this study was Fe-17Mn-5Si-5Cr-0.3C-4Ni-1Ti (mass %). A vacuum induction melting apparatus was used to manufacture the Fe-SMA plate. The Fe-SMA rebar was prepared as follows. (1) The elements of the alloy were put into a vacuum induction melting device and manufactured into an ingot of 1000 kg. (2) A homogenization treatment of the ingot was given for 6 h at 1250 °C. (3) The Fe-SMA plate was manufactured by forging into a plate with a thickness

of 10 mm by a hydraulic press. Finally, (4) the Fe-SMA rebar was manufactured by cutting a 10-mm thick Fe-SMA plate to a width of 100 mm with a water jet.

A direct tensile test was performed to investigate the mechanical properties of the Fe-SMA rebar. For the direct tensile test, the Fe-SMA rebar was machined into a tensile specimen having a thickness of 2.5 mm, a width of 10 mm, and a length of 200 mm. Lee et al. [29] reported that the corrosion resistance of Fe-SMA rapidly decreased when its pre-strain exceeded 0.04. Referring to their research results, the pre-strain of the specimen to evaluate the mechanical properties of the Fe-SMA rebar was set to 0.04. First, the specimen was tensioned with a displacement control of 0.25 mm/min up to a pre-strain of 0.04 by a universal testing machine (UTM) with a capacity of 100 kN. Afterward, the load applied to the specimen was reduced at the same speed until it became zero. A residual strain of 0.032 occurred in the specimen that had undergone a pre-strain of 0.04. The direct tensile test for evaluating the mechanical properties of the pre-strained specimen was performed with a displacement control of 0.5 mm/min using the same equipment. A strain gauge was attached to measure the strain of the specimen during the test, and the measured data were collected at a time interval of 1 s through a data acquisition system (DAQ). Figure 2 shows the stress–strain relationship of the Fe-SMA obtained by the direct tensile test. The modulus of elasticity of the Fe-SMA was 127.3 GPa, and its ultimate strength and elongation were 1035 MPa and 16.8%, respectively.

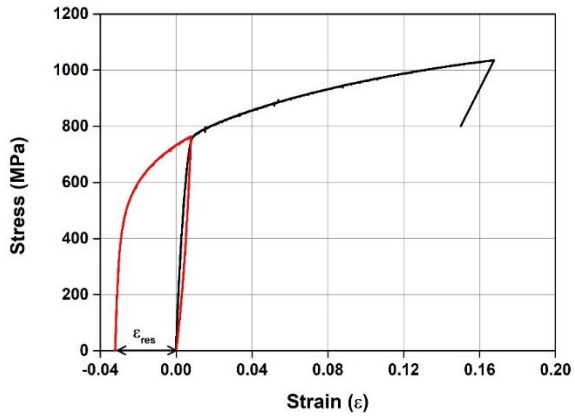

Figure 2. Stress–strain relationship of Fe-SMA rebar.

Figures 3 and 4 show the test set-up for evaluating the recovery stress of Fe-SMA and the strain–temperature–stress relationship of the Fe-SMA rebar in three dimensions, respectively. The X, Y, and Z axes in Figure 4 represent the strain, temperature, and stress of the Fe-SMA specimen, respectively. The specimen used in this test was the same as the specimen used in the direct tensile test. Park et al. [30] reported that ettringite between the cement and aggregates begins to hydrolyze when the temperature of concrete exceeds 160 °C. Yeon [31] reported that when Fe-SMA was heated to a temperature exceeding 160 °C to activate Fe-SMA embedded in mortar, moisture inside the mortar was vaporized, and cracks occurred. Referring to their research results, the heating temperature (T_{max}) of the specimen to evaluate the recovery stress of the Fe-SMA rebar was set to 160 °C. The recovery stress test was performed as follows. (1) The specimen on the 100kN UTM was tensioned to the target pre-strain (ε_{pre}) with a displacement control of 0.25 mm/min (black line in Figure 4). (2) After the strain of the specimen reached 0.04, which was ε_{pre}, the load applied to the specimen was released at 0.25 mm/min until the load on the specimen was set to 0 (green line in Figure 4). (3) To prevent buckling due to the thermal expansion, stress of about 50 MPa was applied to the specimen, and then the displacement of the specimen was constrained. (4) The displacement-constrained specimen was heated up to T_{max} (160 °C) with electrical resistance by supplying a current of 2 A/mm^2 (red line in Figure 4). Finally, (5) when the surface temperature of the specimen reached the target temperature, the power supply was cut off, and it was cooled to room temperature (T_{room})

(blue line in Figure 4). While the Fe-SMA was activated, the temperature of the specimen was measured by an infrared ray heat sensor, as shown in Figure 3, and the measured data were collected at a time interval of 1 s with a DAQ. As shown in Figure 4, when the temperature of the specimen reached about 35 °C at the beginning of heating, its stress was slightly reduced due to thermal expansion. Afterward, the specimen was continuously heated, and when the specimen reached the target temperature, the recovery stress (T_{max}) was about 168 MPa, and when the Fe-SMA specimen was cooled to T_{room}, the recovery stress (σ_{rec}) was about 335 MPa.

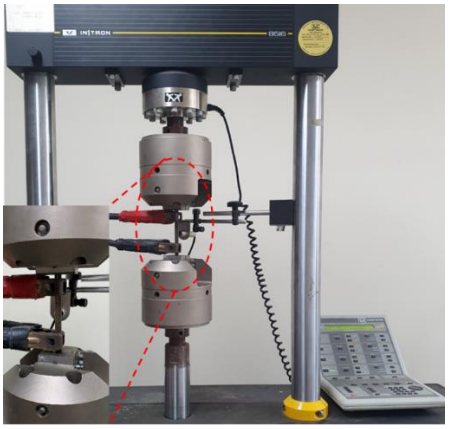

Figure 3. Test set-up for Fe-SMA activation.

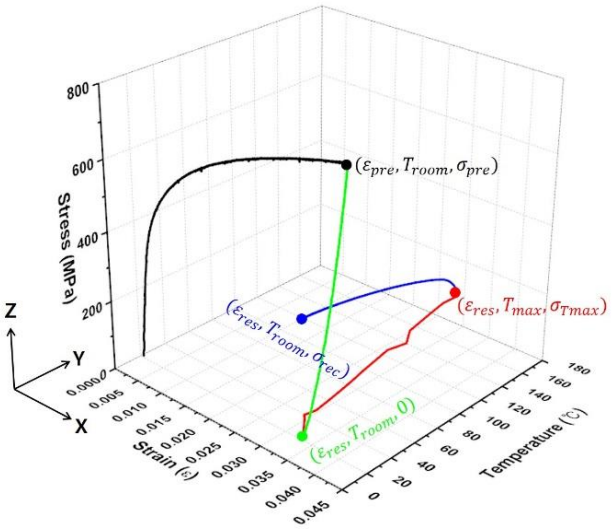

Figure 4. Strain–temperature–stress relationship of Fe-SMA rebar.

2.3. Test Set-Up

As shown in Figure 1, the net span of the concrete slab specimens was 2600 mm, and the Fe-SMA rebars embedded in the specimens were activated by electric resistance heating with an electric power supplier of 5 A/mm^2. As shown in Figure 5, the temperature of the Fe-SMA rebar was measured using an infrared ray heat sensor. It was confirmed through a preliminary experiment that the temperature of the middle section of the Fe-SMA rebar reached the target temperature of 160 °C when the end temperature of the Fe-SMA rebar with a thread reached 440 °C. Accordingly, the power supply was stopped when the surface temperatures of the rebar with and without the thread reached 440 °C and 160 °C, respectively. The camber generated during the activation of the Fe-SMA rebar was measured with a linear variable differential transformer (LVDT) with a capacity of 10 mm,

which was installed on the lower face of the middle of the specimen. Data measured by the thermal sensor and LVDT were collected and stored at a time interval of 1 s using a DAQ.

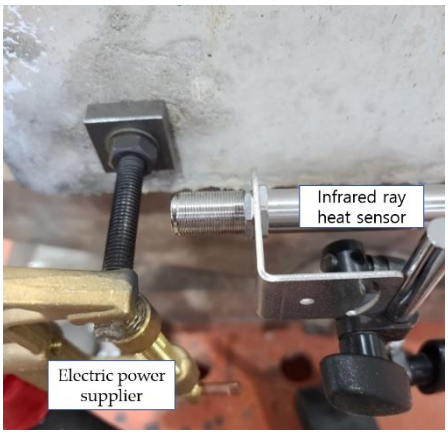

Figure 5. Overview of the activation system.

After displacement of the specimen due to the activation of the Fe-SMA rebar became stable, four-point bending tests to evaluate the flexural behavior of the concrete slab specimens were performed using an actuator with a capacity of 2000 kN. As shown in Figure 1, the distance between the two loading points of the specimen was 400 mm, with each 200 mm from the middle of the specimen to both ends. Displacement-controlled loading was applied at a rate of 3 mm/min. The deflection of the specimen during the loading was measured with two LVDTs with a capacity of 200 mm installed on the lower face of the middle of the specimen, and the initial cracks and crack development that occurred in the specimen during loading were visually observed and recorded on the surface of the specimen. Figure 6 shows the test set-up for the four-point bending test.

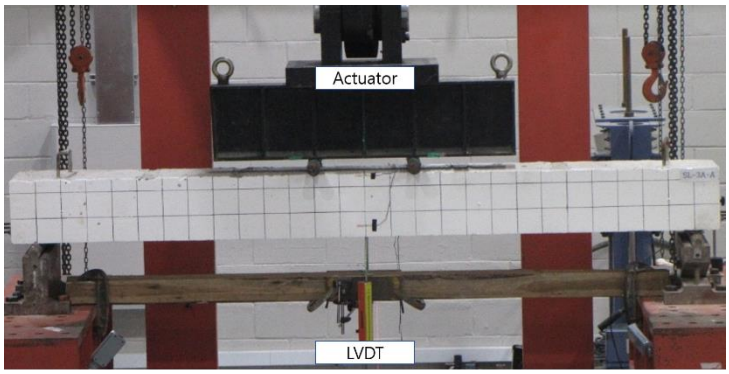

Figure 6. Test set-up.

3. Experiment Results and Discussion

3.1. Activation of Fe-SMA Rebar

Figure 7 shows the time–displacement curve of the middle of the specimen according to the activation of the Fe-SMA rebar. As shown in Figure 7, the time–displacement curve at the middle caused by the activation of the Fe-SMA rebar was clearly divided into two branches. As shown in Figure 7a, at the initial stage of activation, downward displacement occurred in the specimen due to thermal expansion of the Fe-SMA rebar. However, as it was continuously activated, the eccentric compressive force applied to the concrete section gradually recovered the downward displacement due to thermal expansion and finally induced upward displacement (camber), as shown in Figure 7b. The maximum cambers of SL-2A, SL-3A, SL-4A, and SL-5A, according to the activation of the Fe-SMA rebar, were

0.208 mm, 0.301 mm, 0.398 mm, and 0.496 mm, respectively. As the cross-sectional amount of Fe-SMA rebar increased by 100 mm^2, the camber increased by 0.096 mm on average. It was considered that a larger eccentric compressive force was applied to the specimen as the amount of Fe-SMA rebar was increased.

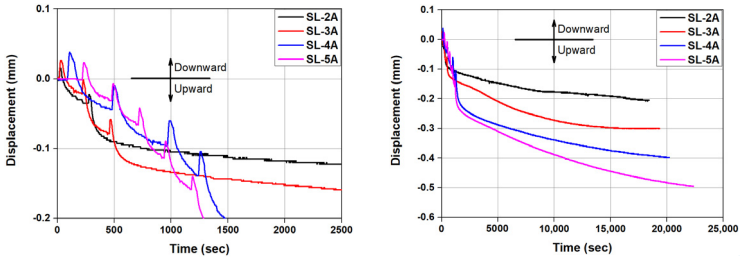

Figure 7. Time–displacement relationship according to amount of Fe-SMA rebar. (**a**) Heating region. (**b**) Cooling region.

3.2. Failure Mode

At the beginning of loading, the initial cracks occurred in the middle zone of all specimens. As the deflection of the specimen increased with the increment of the applied load, the initial crack propagated toward the compression zone. Finally, yielding of the Fe-SMA rebar was followed by crushing of the compressive fiber concrete, and the applied load to the specimen was decreased.

Figure 8 shows the shape of the specimen after the experiment was completed, and Table 3 presents the summarized experimental results. As shown in Figure 8a, four flexural cracks were visually observed in SL-2N, the non-activated test specimen. On the other hand, three flexural cracks were observed in SL-2A, which had the same amount of rebar as SL-2N, and the Fe-SMA rebar was activated. Additionally, by comparing Figure 8a,b, it can be confirmed that the crack distribution width of SL-2N was wider than that of SL-2A. A reduction in both the number of flexural cracks and the crack distribution width according to the activation of the Fe-SMA rebar was also observed in the specimens with different amounts of Fe-SMA rebar. This reduction was considered to be the result of the recovery stress generated in the Fe-SMA rebar by activation, acting as a compressive force on the specimens.

Table 3. Summary of test results.

Specimen	Initial Crack		Ultimate		Failure Mode
	Deflection (mm)	Load (kN)	Deflection (mm)	Load (kN)	
SL-2N	1.45	25.59	87.69	58.66	Flexural
SL-2A	1.42	35.88	89.34	59.05	
SL-3N	1.2	27.73	74.73	92.04	
SL-3A	1.99	46.92	72.59	93.23	
SL-3R	2.35	45.66	79.77	94.87	
SL-4N	0.88	29.06	75.52	117.01	
SL-4A	3.24	52.81	71.53	120.82	
SL-5N	1.00	29.28	96.95	147.91	
SL-5A	2.33	59.03	59.03	148.09	

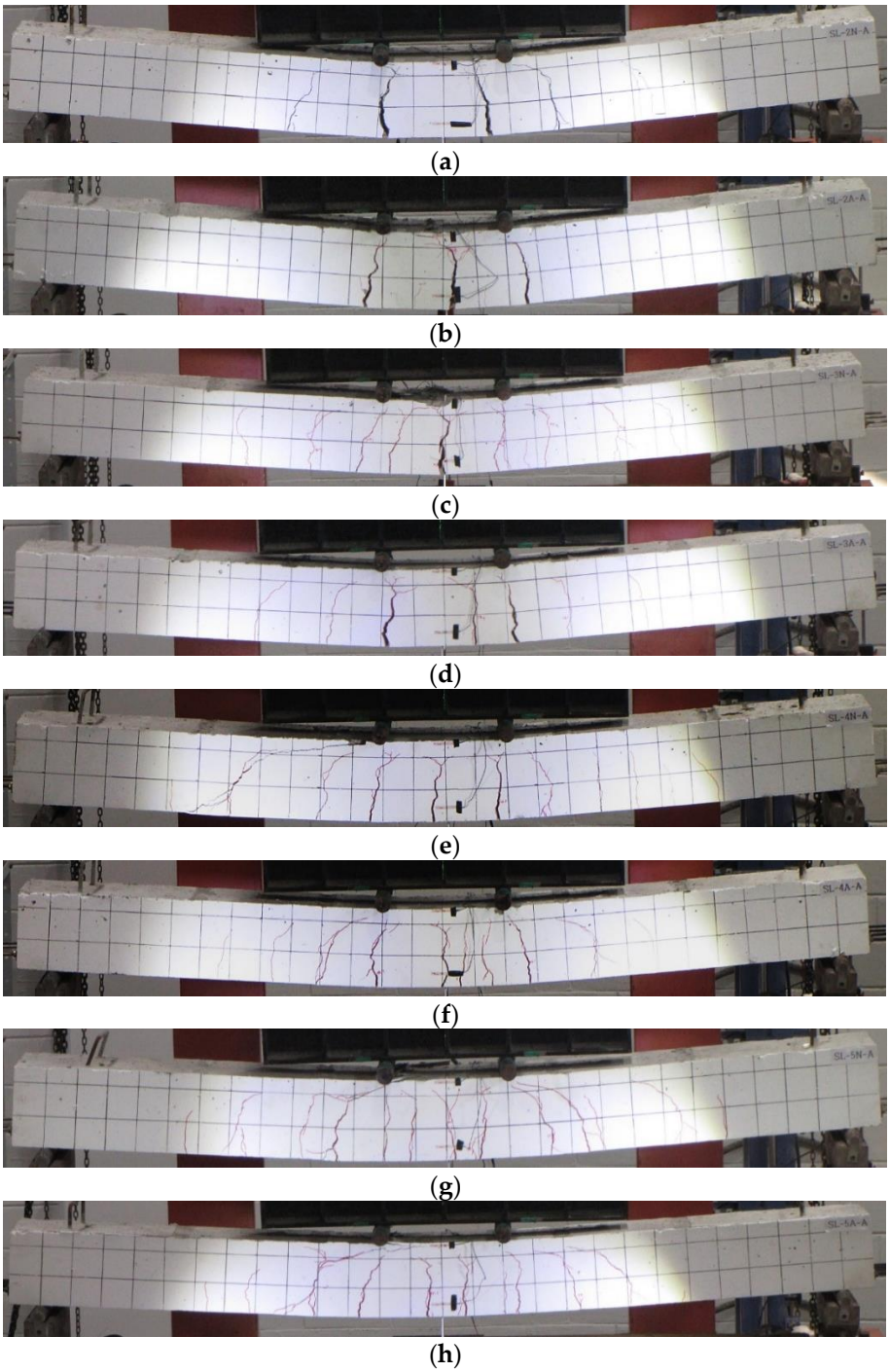

Figure 8. Failure modes of the specimens: (**a**) SL-2N, (**b**) SL-2A, (**c**) SL-3N, (**d**) SL-3A, (**e**) SL-4N, (**f**) SL-4A, (**g**) SL-5N, and (**h**) SL-5A.

3.3. Load–Fe-SMA Rebar Strain Relationship

Figure 9 shows a comparison of the load–Fe-SMA rebar strain relationship of the specimens in which the Fe-SMA was not activated. The strain of the Fe-SMA rebar was measured by a strain gauge attached to the middle of the rebar. The strain of the specimen with the activated Fe-SMA rebar was not measured due to damage to the strain gauge during electrical resistance heating. As shown in Figure 9, the strain of the Fe-SMA rebar increased rapidly after cracking in the concrete. This was because of the material that resisted external load changes from concrete to rebar after cracking.

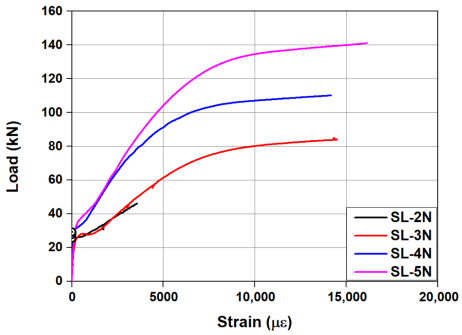

Figure 9. Comparison of load–Fe-SMA rebar strain curves of non-activated specimens according to area of Fe-SMA rebar.

3.4. Load–Deflection Relationship

3.4.1. Effect of the Fe-SMA Rebar Activation

Figure 10 shows a comparison of the load–displacement relationship between the non-activated specimens and activated specimens. As shown in Figure 10a, the initial crack of SL-2N, in which the Fe-SMA rebar was not activated, occurred at a load of 25.59 kN, whereas the initial crack of SL-2A, in which the Fe-SMA rebar was activated, occurred at a load of 35.88 kN, which was 40.2% higher than that of SL-2N. In addition, the initial crack loads of SL-3A, SL-4A, and SL-5A, where the Fe-SMA rebar was activated, were 69.2%, 81.7%, and 101.6% larger than those of SL-3N, SL-4N, and SL-5N, where the Fe-SMA rebar was non-activated, respectively. As shown in Figure 10, the stiffness of the specimen in which the Fe-SMA rebar was activated was greater than that of the specimen in which the Fe-SMA rebar was not activated. For example, the deflection of SL-2N and SL-2A at 50 kN was 18.82 mm and 15.54 mm, respectively, and the deflection of SL-2A was about 17% smaller than that of SL-2N. In addition, the deflection of SL-3N and SL-3A at 50 kN was 8.68 mm and 3.52 mm, respectively. The deflection of SL-3A was about 59% smaller than that of SL-3N. The larger initial cracking loads and stiffness of the activated specimens than those of the non-activated specimens are thought to be attributable to the recovery stress generated by rebar activation acting as a compressive force on the specimen. On the other hand, the ultimate load of the specimens with the same amount of Fe-SMA bar was only slightly different, changing in a range of 0.12–3.15% regardless of activation of the Fe-SMA rebar. Therefore, similar to conventional prestressed concrete, it can be confirmed that the effect of the prestressing force due to Fe-SMA activation on the ultimate load of the reinforced concrete member was negligible. It can also be confirmed through the experimental results that activation of the Fe-SMA rebar was more effective in terms of improving usability, such as improvement of initial crack load and initial stiffness, rather than improvement of the strength of the member reinforced with Fe-SMA rebar.

3.4.2. Effect of the Amount of Fe-SMA Rebar

Figure 11 presents a comparison of the load–displacement relationship of the specimen according to an increase in the amount of Fe-SMA rebar. As shown in Figure 11a, the initial crack loads of SL-2N, SL-3N, SL-4N, and SL-5N, wherein the Fe-SMA rebar was not activated, were 25.59 kN, 27.73 kN, 29.06 kN, and 29.28 kN, respectively. When the amount of Fe-SMA rebar was increased by 100 mm^2, the initial crack load increased slightly (by 4.63% on average). As shown in Figure 11a, when the amount of the Fe-SMA rebar was increased, the flexural stiffness was significantly improved after initial cracking. The ultimate loads of SL-2N, SL-3N, SL-4N, and SL-5N were 58.66 kN, 92.04 kN, 117.01 kN, and 147.91 kN, respectively, and when the amount of the Fe-SMA rebar was increased by 100 mm^2, the ultimate load increased linearly by approximately 30 kN on average. Therefore, the initial cracking load of the member without the activated Fe-SMA rebar was not significantly affected by the amount of Fe-SMA rebar, but the ultimate load was significantly affected. Figure 11b shows a comparison of the load–displacement

relationship of the activated specimens according to the increase in the amount of Fe-SMA rebar. The initial crack loads of the activated specimens SL-2A, SL-3A, SL-4A, and SL-5A were 35.88 kN, 46.92 kN, 52.81 kN, and 59.03 kN, respectively. Unlike the non-activated specimens, when the amount of the Fe-SMA rebar was increased by 100 mm^2, the initial crack load increased by an average of 18.4%. In addition, as the amount of the Fe-SMA rebar was increased, the stiffness of the specimens increased remarkably after the initial crack occurred. In the case of the activated specimens, when the amount of the Fe-SMA rebar was increased by 100 mm^2, the ultimate load increased by about 29 kN, similar to that of the non-activated specimens.

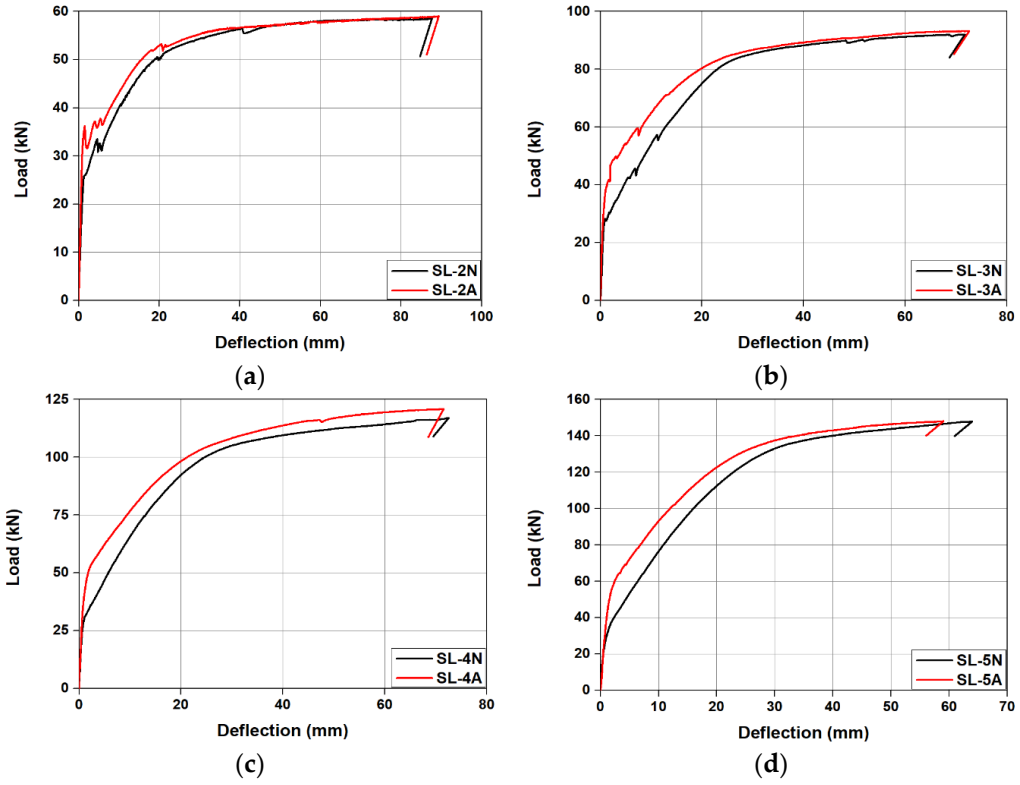

Figure 10. Comparison of load–deflection curves according to activation of Fe-SMA rebar: (**a**) SL-2N and SL-2A, (**b**) SL-3N and SL-3A, (**c**) SL-4N and SL-4A, and (**d**) SL-5N and SL-5A.

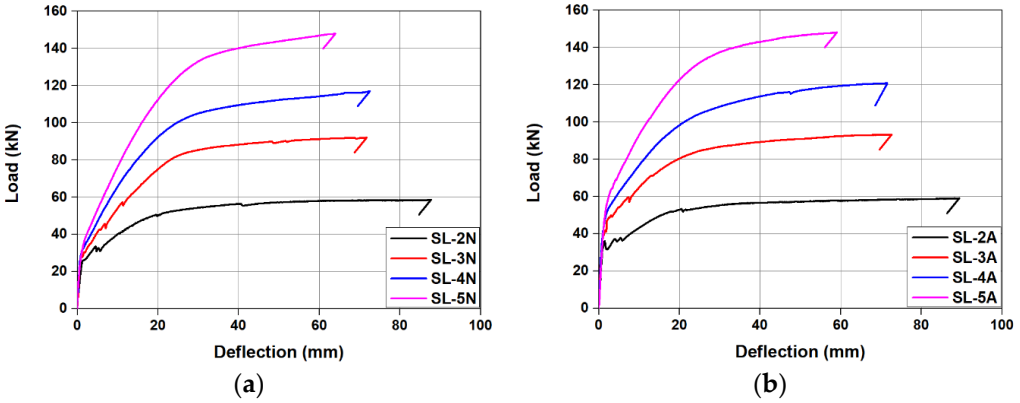

Figure 11. Comparison of load–deflection curves according to amount of Fe-SMA rebar. (**a**) Non-activated specimens. (**b**) Activated specimens.

The initial cracking moment (M_{cr}) is the moment that makes the tensile stress of the outermost fiber of the concrete cross-section equal to the flexural tensile strength (f_{cr}) of the concrete.

The internal stresses of the concrete member with Fe-SMA rebar subjected to external load are composed of the compressive stress (f_{c1}) generated by the recovery stress of Fe-SMA, the flexural stress (f_{c2}) generated by the eccentric compressive force, and the flexural stress (f_{c3}) generated by an external load. These three stresses in the outermost concrete fiber below the neutral axis can be expressed as Equations (1)–(3), respectively. The sum of the bending stresses (f_c) in the outermost concrete fibers below the neutral axis can be expressed as Equation (4). The compressive force (P_{rec}) generated by the activation of the Fe-SMA rebar of Equation (1) can be calculated through Equation (5), and the recovery stress (f_{rec}) of the Fe-SMA rebar of 335 MPa was used based on the experimental results:

$$f_{c1} = \frac{P_{rec}}{A_c} \tag{1}$$

$$f_{c2} = \frac{P_{rec} \times e}{I_g} y \tag{2}$$

$$f_{c3} = -\frac{M_a}{I_g} y \tag{3}$$

$$f_c = f_{c1} + f_{c2} + f_{c3} \tag{4}$$

$$P_{rec} = f_{rec} A_{sma} \tag{5}$$

where A_c is the area of the concrete section, e is the eccentric distance, and A_{sma} is the area of the Fe-SMA rebar. In addition, y represents the distance from the outermost concrete fiber to the neutral axis, M_a is the moment applied to the member by an external load, and I_g is the moment of inertia of the specimen.

In ACI 318 [32], f_{cr} is defined via Equation (6). Therefore, by assuming that the flexural stress in the outermost concrete fiber below the neutral axis in Equation (4) is equal to the flexural tensile strength of the concrete, and that the moment generated by an external load is equal to the initial cracking moment, the initial crack moment and the initial crack load (P_{cr}) can be obtained from Equations (7) and (8), respectively:

$$f_{cr} = 0.63\sqrt{f\prime_c} \tag{6}$$

$$M_{cr} = \frac{f_{cr} I_g}{y} + \frac{P_{rec} I_g}{A_c y} + P_{rec} \times e \tag{7}$$

$$P_{cr} = \frac{2M_{cr}}{a} \tag{8}$$

where $f\prime_c$ is the compressive strength of concrete and a is the distance from the support point to the load point.

Figure 12 shows a comparison between the theoretical initial crack load ($P_{cr,theory}$) calculated from Equations (1)–(8) and the experimental initial crack load ($P_{cr,exp}$). The theoretical initial crack loads of SL-2A, SL-3A, SL-4A, and SL-5A calculated by these formulas were 47.87 kN, 55.59 kN, 63.30 kN, and 71.02 kN, respectively. The ratio of the theoretical value to the experimental value was calculated to have an average value of 0.81. The experimental value was smaller than the theoretical value for the following two reasons. This first was the thermal expansion of the Fe-SMA rebar interfacial concrete during activation of the Fe-SMA rebar. Hosseini et al. [27] reported that when thermal expansion of the matrix occurred, the recovery stress of Fe-SMA was reduced by about 50% compared with that of Fe-SMA under the ideal constraint condition. In addition, they argued that the reduction in the recovery stress of the Fe-SMA due to thermal expansion of the matrix should be minimized by heating the Fe-SMA as soon as possible during Fe-SMA activation. Although the Fe-SMA rebar heating time was as short as 30 s in this study, it was considered that thermal expansion occurred in the concrete surrounding the interface of the Fe-SMA rebar. Therefore, additional studies are required in the future to quantitatively evaluate the thermal expansion of the interfacial concrete and the corresponding decrease

in the recovery stress of Fe-SMA during activation of the Fe-SMA rebar. The second cause may be some activation of the Fe-SMA rebar by the heat of hydration of concrete during curing of the concrete. According to ACI, concrete with a compressive strength of 41.4 MPa (6000 psi) or more is classified as high-strength concrete [33]. High-strength concrete is known to have a relatively high heat of hydration due to the use of a large amount of cement [34]. The compressive strength of the concrete used in this study was 46.2 MPa, and it was thus classified as high-strength concrete. Therefore, it was judged that a relatively high heat of hydration occurred during concrete curing. Accordingly, when Fe-SMA rebar is applied to high-strength concrete members, appropriate measures are required to reduce the concrete hydration heat.

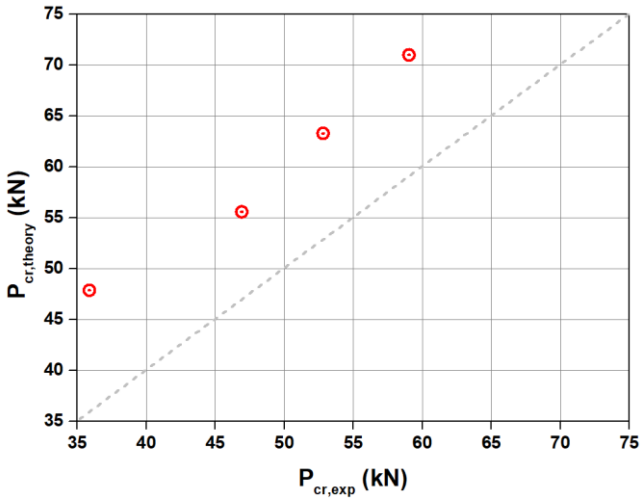

Figure 12. Comparison of $P_{cr,exp}$ and $P_{cr,theory}$.

3.4.3. Reactivation of Fe-SMA Rebar

As mentioned earlier, the prestressed concrete member with the SMA rebar has the advantage of being able to recover the prestress force (recovery force), even though it is a bonded prestressed concrete in which the Fe-SMA rebar and the concrete work integrally. To verify this, a reactivation experiment of Fe-SMA rebar was performed on the SL-3R specimen. This test was performed by repeating the following steps four times. (1) The Fe-SMA rebar of the specimen was activated in the same way as described in Section 2.3. (2) The specimen was loaded up to 70% of the ultimate load of the activated specimen (however, the last (fourth) loading was carried out until the specimen was destroyed). Finally (3), the load applied to the specimen was reduced to 0 for about 1 min.

Figure 13 shows the time–upward displacement relationship in the middle of the specimen during Fe-SMA activation and reactivation. A camber of 0.314 mm occurred during the first activation of the SL-3R specimen without preloading. In the SL-3R, which was loaded up to a load corresponding to 70% of its ultimate load, a camber of 1.08 mm, 0.954 mm, and 0.987 mm was generated during the second, third, and fourth activations, respectively. These values were 344%, 304%, and 314% larger than the camber generated in the first activation, respectively. The camber was larger in the second, third, and fourth activations than in the first activation because the flexural stiffness of the cross section was greatly reduced due to the cracks generated in the specimen as a result of the pre-loading.

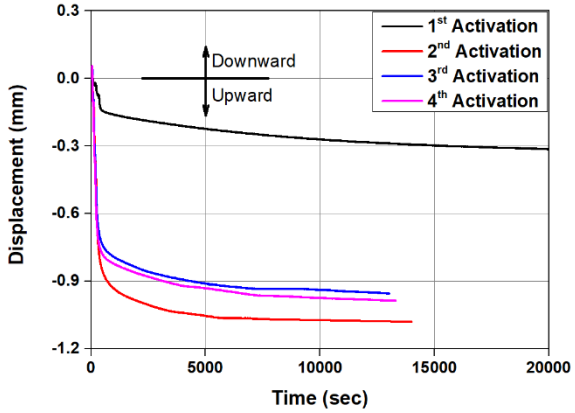

Figure 13. Time–displacement relationship of SL-3R according to number of activations.

Figure 14 shows a comparison of the load–displacement relationship between the SL-3R, where the Fe-SMA rebar was activated four times, and the SL-3A. As shown in Figure 13, in the SL-3R specimen, where a load of 70% of the ultimate load was applied, residual deflection occurred even when the load was removed, and a portion of the deflection was recovered by the activation of the Fe-SMA. After the fourth Fe-SMA rebar's activation was completed, the specimen was loaded until it was destroyed. As can be seen from Figure 14, the load–displacement relationship of SL-3R was similar to that of specimen SL-3A, which was activated once, regardless of the number of activations. The ultimate load of SL-3R, which had undergone four activations, was only 1.8% different from that of the SL-3A. Therefore, it can be concluded that the effect of the number of activations on the flexural behavior of the member is very insignificant.

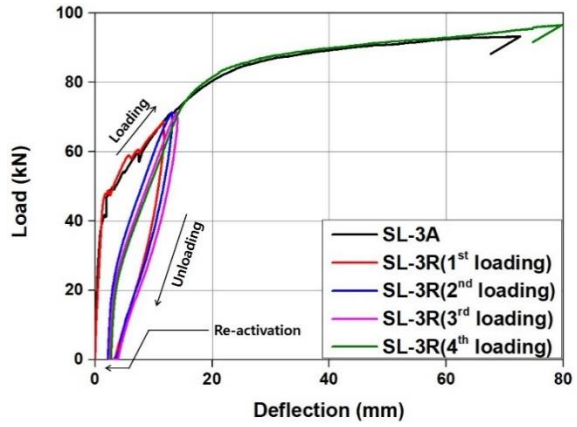

Figure 14. Comparison of load–deflection relationship between SL-3A and SL-3R.

It is considered that the prestress force of the concrete reinforced with Fe-SMA rebar can be recovered through reactivation even if the prestress force is reduced due to various reasons, such as drying shrinkage and relaxation, unlike conventional bonded prestressed concrete. Therefore, it is judged that the self-prestressing method through Fe-SMA rebar can solve the disadvantages of the low strength problem of unbonded prestressed concrete and the difficulty of retensioning bonded prestressed concrete.

4. Conclusions

In this paper, an experimental study was conducted to evaluate the flexural behavior of self-prestressed concrete slabs with Fe-SMA rebar, and the following conclusions were drawn:

1. Activation of the Fe-SMA rebar caused camber in the concrete member by applying an eccentric compressive force due to the recovery stress on the cross-section. This camber

increased by an average of 0.096 mm when the amount of Fe-SMA reinforcement increased by 100 mm^2.

2. The initial cracking load of the specimen with the activated Fe-SMA rebar was 40~101% greater than that of the non-activated specimen due to the action of the eccentric compressive load.
3. The theoretically calculated initial crack load was 23% larger on average compared with the experimental value. This was considered to be due to the reduction of the recovery stress resulting from the thermal expansion at the Fe-SMA and concrete interface and the concrete hydration heat. Therefore, future studies are needed to quantitatively evaluate the effect of thermal expansion and hydration heat of concrete on the recovery stress of Fe-SMA rebar.
4. The effect of the Fe-SMA rebar activation on the ultimate load of the concrete member was negligible. Therefore, it was confirmed that the introduction of prestress by activation of the Fe-SMA rebar, like traditional prestressed concrete, mainly increased the usability of the concrete member.
5. The load–displacement relationship of the specimen with Fe-SMA rebars activated four times was similar to that of the specimen with Fe-SMA rebars activated once. Therefore, it was considered that the prestress force of the concrete reinforced with Fe-SMA rebar could be recovered through reactivation even if the prestress force was reduced due to various reasons, such as drying shrinkage and relaxation, unlike the conventional bonded prestressed concrete.
6. Through this study, it was confirmed that the concrete prestressing method using the Fe-SMA rebar could solve several disadvantages of conventional prestressed concrete. Therefore, the self-prestressing method using Fe-SMA was expected to have high potential in the field of prestressed concrete for new construction.

Author Contributions: K.-N.H. and Y.-M.Y. conceptualized the study; Y.-M.Y. obtained field data; Y.-M.Y. and S.-W.J. implemented data processing under the supervision of K.-N.H.; the original draft of the manuscript was written by K.-N.H. and Y.-M.Y. with editorial contributions from S.-W.J. All authors have read and agreed to the published version of the manuscript.

Funding: This research was funded by a National Research Foundation of Korea (NRF) grant funded by the Korea government (MSIT), grant number 2020R1A2C1003197.

Acknowledgments: This work was supported by the National Research Foundation of Korea (NRF) grant funded by the Korea government (MSIT) (2020R1A2C1003197).

Conflicts of Interest: The authors declare no conflict of interest.

References

1. Lee, D.-K.; Han, S.-J.; Joo, H.-E.; Kim, K.-S. Control of tensile stress in prestressed concrete members under service loads. *Int. J. Concr. Struct. Mater.* **2017**, *12*, 425–437. [CrossRef]
2. Silva, S.-D.; Mutsuyoshi, H.; Witchukrenangkrai, E. Evaluation of shear crack width in I-shaped prestressed reinforced concrete beams. *J. Adv. Concr. Technol.* **2008**, *6*, 443–458. [CrossRef]
3. Zhao, Y.; Zhou, Y.; Feng, C.; Liu, Z.; He, Z. Experimental and simulation analysis of prestressed concrete continuous box girder bridge. *Rev. Tec. Ing. Univ. Zulia* **2016**, *39*, 392–398.
4. Caro, L.A.; Martí-Vargas, J.R.; Serna, P. Prestress losses evaluation in prestressed concrete prismatic specimens. *Eng. Struct.* **2013**, *48*, 704–715. [CrossRef]
5. Lee, D.-S.; Kim, T.-K.; Lee, S.-C. Development and field application of portable tensioning system using segmental CFT member. *J. Korean Soc. Civ. Eng.* **2014**, *34*, 965–975. [CrossRef]
6. Hong, S. Effect of prestress levels and jacking methods on friction losses in curved prestressed tendons. *Appl. Sci.* **2017**, *7*, 824. [CrossRef]
7. Pischulev, A.; Panfilov, D.; Zhiltsov, Y. Experimental investigation of reinforced concrete beams using post-tension. In *IOP Conference Series: Materials Science and Engineering*; IOP Publishing: Bristol, UK, 2020.
8. Abdelhalim, J. Prestressed Concrete Slabs with Bonded and Unbonded Tendons. Master' Thesis, The American University in Cairo, Cairo, Egypt, 2021.
9. Sun, X.-T.; He, W.-Y.; Wang, Z.-C.; Ren, W.-X. Grouting quality evaluation in post-tensioning tendon ducts using wavelet packet transform and bayes classifier. *Sensors* **2019**, *19*, 5372. [CrossRef]

10. Gu, X.; Jin, X.; Zhou, Y. *Prestressed Concrete Structures*; Springer: Berlin/Heidelberg, Germany, 2016; pp. 415–495. [CrossRef]
11. Abdullah, A.B.M.; Rice, J.A.; Hamilton, H.R. Wire breakage detection using relative strain variation in unbonded posttensioning anchors. *J. Bridge Eng.* **2015**, *20*, 04014056. [CrossRef]
12. Yoon, I.-S.; Kang, H.-K.; Shin, H.-Y. Evaluation of corrosion prevention systems of strands for PSC structures. *J. Korea Concr. Inst.* **2019**, *31*, 557–565. [CrossRef]
13. Rojob, H.; El-Hacha, R. Self-prestressing using iron-based shape memory alloy for flexural strengthening of reinforced concrete beams. *ACI Struct. J.* **2017**, *114*, 523–532. [CrossRef]
14. Debska, A.; Gwozdziewicz, P.; Seruga, A.; Balandraud, X.; Destrebecq, J.F. Prestress state evolution during thermal activation of memory efect in concrete beams strengthened with external SMA wire. *Arch. Civ. Mech. Eng.* **2020**, *20*, 142. [CrossRef]
15. Hong, K.-N.; Yeon, Y.-M.; Shim, W.-B.; Kim, D.-H. Recovery behavior of Fe-based shape memory alloy under different restraints. *Appl. Sci.* **2020**, *10*, 3441. [CrossRef]
16. Lee, W.J.; Weber, B.; Leinenbach, C. Recovery stress formation in a restrained Fe–Mn–Si-based shape memory alloy used for prestressing or mechanical joining. *Constr. Build. Mater.* **2015**, *95*, 600–610. [CrossRef]
17. Kim, M.-S. Mechanical Properties and Shape Memory Properties of Ti50Ni50/Ti50Ni35Cu15 Functionally Graded Shape Memory. *Sci. Adv. Mater.* **2015**, *12*, 1586–1590. [CrossRef]
18. Buehler, W.J.; Gilfrich, L.V.; Wiley, R.C. Effect of Low Temperature Phase Changes on the Mechanical Properties of Alloys Near Composition TiNi. *J. Appl. Phys.* **1963**, *34*, 1475–1477. [CrossRef]
19. Yun, J.-H. Deterministic and Probabilistic Assessment of Seismic Performance of Bridges Retrofitted with Shape Memory Alloy. Doctoral Dissertation, Hanyang University, Seoul, Korea, 2008.
20. Michels, J.; Shahverdi, M.; Czaderski, C. Flexural strengthening of structural concrete with iron-based shape memory alloy strips. *Struct. Concr.* **2018**, *19*, 876–891. [CrossRef]
21. Shahverdi, M.; Czaderski, C.; Motavalli, M. Iron-based shape memory alloys for prestressed near-surface mounted strengthening of reinforced concrete beams. *Constr. Build. Mater.* **2016**, *112*, 28–38. [CrossRef]
22. Shahverdi, M.; Michels, J.; Czaderski, C.; Motavalli, M. Iron-based shape memory alloy strips for strengthening RC members: Material behavior and characterization. *Constr. Build. Mater.* **2018**, *173*, 586–599. [CrossRef]
23. Abouali, S.; Shahverdi, M.; Ghassemieh, M.; Motavalli, M. Nonlinear simulation of reinforced concrete beams retrofitted by near surface mounted iron based shape memory alloy. *Eng. Struct.* **2019**, *187*, 133–148. [CrossRef]
24. Hong, K.-N.; Lee, S.-G.; Han, S.-H.; Yeon, Y.-M. Evaluation of Fe-based shape memory alloy (Fe-SMA) as strengthening material for reinforced concrete structures. *Appl. Sci.* **2016**, *8*, 730. [CrossRef]
25. Kim, D.; Kim, Y.; Oak, J.-J.; Lee, J.; Park, C.-H.; Lee, W.; Park, Y. Effect of Ni, C and Ti addition on shape recovery behavior and the mechanical properties of Fe-17Mn-5Si-5Cr shape memory alloy. *Korean J. Met. Mater.* **2020**, *58*, 660–671. [CrossRef]
26. Yeon, Y.-M.; Hong, K.-N.; Shim, W.-B. Iron-based shape memory alloy strips for strengthening RC members: Material behavior and characterization Long-term behaivor of reinforced concrete beams strengthened with near-surface mounted Fe-based shape memory alloy strips. *J. Korean. Soc. Adv. Comp. Struc.* **2020**, *11*, 11–17. [CrossRef]
27. Hosseini, E.; Ghafoori, E.; Leinenbach, C.; Motavalli, M.; Holdsworth, S.R. Stress recovery and cyclic behaviour of an Fe–Mn–Si shape memory alloy after multiple thermal activation. *Smart Mater. Struct.* **2018**, *27*, 025009. [CrossRef]
28. *ASTM C39/C39M-17*; Standard Test Method for Compressive Strength of Cylindrical Concrete Specimens. ASTM International: West Conshohocken, PA, USA, 2017.
29. Lee, W.-J.; Partovi-Nia, R.; Suter, T.; Leinenbach, C. Electrochemical Characterization and Corrosion Behavior of an Fe-Mn-Si Shape Memory Alloy in Simulated Concrete Pore Solutions. *Mater. Corros.* **2015**, *67*, 839–846. [CrossRef]
30. Park, S.-J.; Yim, H.-J.; Kwak, H.-G. Evaluation of microcracks in thermal damaged concrete using nonlinear ultrasonic modulation technique. *J. Korea Concr. Inst.* **2012**, *24*, 651–658. [CrossRef]
31. Yeon, Y.-M. Evaluation of Prestressing Effect for Fe-Based Shape Memory Alloy. Master Thesis, Chungbuk National University, Cheongju, Korea, 2018.
32. ACI. *Building Code Requirements for Structural Concrete*; ACI 318-08; ACI: Farmington Hills, MI, USA, 2008.
33. Santhanam, N.; Anbuarasu, G. Experimental Study on High Strength Concrete (M60) with Reused E-Waste Plastics. *Mater. Today Proceed.* **2019**, *22*, 919–925. [CrossRef]
34. Jaung, J.-D.; Cho, H.-D.; Park, S.-W. Properties of hydration heat of high-strength concrete and reduction strategy for heat production. *J. Korea Insititute Build. Constr.* **2012**, *12*, 203–210. [CrossRef]